Plaquette Singlet Transition, Magnetic Barocaloric Effect, and Spin Supersolidity in the Shastry-Sutherland Model

Junsen Wang,[1,2,*] Han Li,[3,2,*] Ning Xi,[2] Yuan Gao,[4,2] Qing-Bo Yan,[1,†] Wei Li,[2,5,6,‡] and Gang Su[3,5,§]

[1]Center of Materials Science and Optoelectronics Engineering, College of Materials Science and Opto-electronic Technology, University of Chinese Academy of Sciences, Beijing 100049, China

[2]CAS Key Laboratory of Theoretical Physics, Institute of Theoretical Physics, Chinese Academy of Sciences, Beijing 100190, China

[3]Kavli Institute for Theoretical Sciences, University of Chinese Academy of Sciences, Beijing 100190, China

[4]School of Physics, Beihang University, Beijing 100191, China

[5]CAS Center for Excellence in Topological Quantum Computation, University of Chinese Academy of Sciences, Beijing 100190, China

[6]Hefei National Laboratory, University of Science and Technology of China, Hefei 230088, China

(Received 26 February 2023; accepted 16 August 2023; published 14 September 2023)

Inspired by recent experimental measurements [Guo *et al.*, Phys. Rev. Lett. **124**, 206602 (2020); Jiménez *et al.*, Nature (London) **592**, 370 (2021)] on frustrated quantum magnet $SrCu_2(BO_3)_2$ under combined pressure and magnetic fields, we study the related spin-1/2 Shastry-Sutherland model using state-of-the-art tensor network methods. By calculating thermodynamics, correlations, and susceptibilities, we find, in zero magnetic field, not only a line of first-order dimer-singlet to plaquette-singlet phase transition ending with a critical point, but also signatures of the ordered plaquette-singlet transition with its critical end point terminating on this first-order line. Moreover, we uncover prominent magnetic barocaloric responses, a novel type of quantum correlation induced cooling effect, in the strongly fluctuating supercritical regime. Under finite fields, we identify a quantum phase transition from the plaquette-singlet phase to the spin supersolid phase that breaks simultaneously lattice translational and spin rotational symmetries. The present findings on the Shastry-Sutherland model are accessible in current experiments and would shed new light on the critical and supercritical phenomena in the archetypal frustrated quantum magnet $SrCu_2(BO_3)_2$.

DOI: 10.1103/PhysRevLett.131.116702

Introduction.—Frustrated magnetism constitutes a fertile ground breeding enriched spin states and phase transitions [1,2], including unusual spin orders, quantum spin liquid [3–5], and unconventional quantum critical point (QCP) like the deconfined QCP (DQCP) [6], etc. The paradigmatic Shastry-Sutherland (SS) model is a highly frustrated quantum spin system with an analytically known ground state in certain parameter regime [7]. Nevertheless, its global phase diagram hosts rich spin states and transitions, where numerical simulations are playing an increasingly important role [8–25]. On the other hand and as a miracle of nature, the SS model is faithfully realized by a quantum magnetic material $SrCu_2(BO_3)_2$ whose pressure-field-temperature phase diagram is under intensive investigation [26–34], and the intriguing magnetic phenomena observed in experiments in turn require further theoretical studies of the SS model.

The spin-1/2 SS model is defined on a square lattice with the Hamiltonian

$$H = J\sum_{\langle i,j\rangle} \mathbf{S}_i \cdot \mathbf{S}_j + J'\sum_{\langle\langle i,j\rangle\rangle} \mathbf{S}_i \cdot \mathbf{S}_j, \tag{1}$$

where $J > 0$ is the antiferromagnetic (AFM) coupling on the interdimer, and $J' > 0$ on the intradimer bonds [cf. Fig. 1(b)]. We take $J' = 1$ as the energy scale hereafter. For $\alpha \equiv J/J' \leq 0.5$, the ground state is rigorously a product of singlets on the J' dimers [7], dubbed the dimer-singlet (DS) phase. While for the other limit, $\alpha \gg 1$, it has clearly a Néel AFM state [35], and possible intermediate phases were debated for decades [8–17]. Now a consensus has more or less been reached that there exists an intervening plaquette-singlet (PS) phase [18–25,28,30,32,33]. The DS-PS transition is first order, while the PS-AFM transition is possibly second order and belongs to a DQCP [20]. Evidence of the intermediate PS phase and pressure-induced quantum phase transitions (QPTs) were indeed found in recent experiments [28,30,31].

However, there are still enigmas surrounding this seemingly innocent PS phase. For example, the experiments on $SrCu_2(BO_3)_2$ show that the plaquette singlets sit on "full" plaquettes containing diagonal bonds [28,32,47]; while recent ground-state numerics suggest the "empty" plaquettes without diagonal bonds instead [18,20–25]. As a crucial step toward resolving this discrepancy, a finite-temperature calculation from the theoretical side is much in demand first: how about the competition between the instabilities toward empty and full PS order across the full temperature range? After all, based only on the

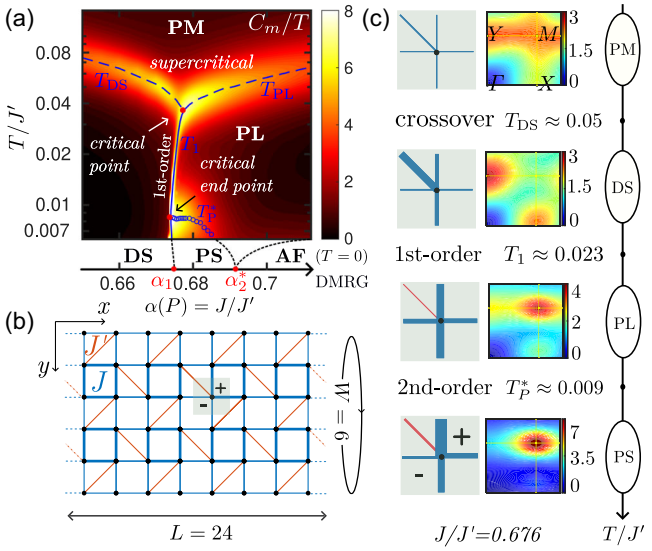

FIG. 1. (a) Pressure-temperature phase diagram of the SS model with magnetic specific heat C_m/T as contour background. The low-temperature data smoothly extrapolate to the ground-state results, where a first-order QPT occurring at $\alpha_1 \simeq 0.673$ and a QCP at $\alpha_2^* \simeq 0.692$ are obtained by DMRG [36] on the same geometry. Two crossovers T_{DS} and T_{PL} (blue dashed lines), first-order T_1 (solid line), and second-order transition T_P^* (empty circle for each data point) are determined from peaks of C_m/T. (b) The 6×24 cylinder with the ordered PS phase illustrated. (c) Temperature evolution of local bond correlators (first column), static spin structure factors (second column), and the corresponding phases (third column) for $J/J' = 0.676$. Local correlators are measured at the center of the lattice, exemplified by the light green square in (b), with two types of empty plaquettes indicated by $+$ and $-$ signs, respectively. Blue (red) bonds indicate negative (positive) correlations with their widths proportional to the absolute values.

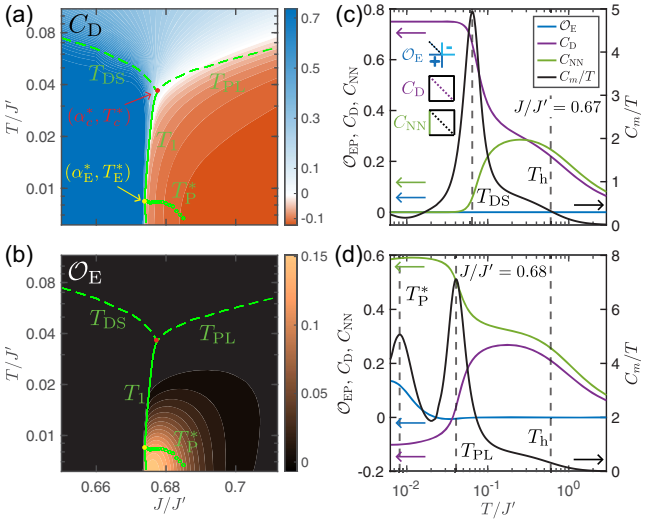

FIG. 2. Contour plots of (a) intradimer correlator C_D and (b) order parameter $\mathcal{O}_E$ for the empty PS order. Green dashed, solid, and dotted lines are peaks of C_m/T, and red (yellow) dot represents the CP (CEP) [cf. Fig. 1(a)]. (c), (d) Magnetic specific heat C_m/T, in conjunction with C_D, interdimer correlator C_{NN}, and $\mathcal{O}_E$ vs T, for $J/J' = 0.67$ and 0.68, respectively. The inset in (c) illustrates definitions of these quantities. Roughly 6% total entropy is released near the T_P^* peak, consistent with experimental result of ~4% obtained at 1.8 GPa [30].

ground-state results one cannot exclude in principle a full-plaquette phase at an intermediate temperature. Recent specific heat measurements on $SrCu_2(BO_3)_2$ found a signal at $T \sim 2$ K, conjecturing that it reflects the onset of PS order [30,31]. Despite great efforts for thermodynamics simulations made in recent years [21,48,49], this signal remains elusive theoretically due to the great challenges in unbiased calculations down to such low temperature.

In this work, we perform a finite-temperature study of the SS model on a cylinder geometry with the state-of-the-art exponential tensor renormalization group (XTRG) approach [50–52]. XTRG has been successfully used in studying frustrated quantum magnets [53–56], and here we simulate the SS model down to $T/J' \sim 0.006$ on a long cylinder. By mapping out the phase diagram, we reproduce the critical point [31] and uncover the empty PS phase below the thermal transition line T_P^* with a $\mathbb{Z}_2$ symmetry breaking. Although the calculations are restricted within $W = 6$ cylinders, we believe the conclusions also hold for wider ones (preliminary width-8 results also support this scenario, see Supplemental Material, Fig. S2 [36]), and therefore explain the specific heat peak observed at $T \lesssim 2$ K in recent experiments [30,31]. We further propose a pronounced quantum correlation cooling driven by pressure (that controls the coupling ratio α) in the supercritical regime. As a companion, we also perform density-matrix renormalization group (DMRG) [57] calculations to explore the QPTs driven by combined pressure and magnetic fields. In particular, evidence for the QPT between the PS phase and a spin supersolid (SSS) phase is witnessed, whose location well agrees with recent experiments [32].

The SS model phase diagram.—The obtained pressure-temperature phase diagram of the SS model is shown in Fig. 1(a) based on the contour plot of the magnetic specific heat C_m/T. As the first-order transition line is slightly bent, one goes over various spin states as temperature decreases with fixed $J/J' = 0.676$, and find in Fig. 1(c) intriguing temperature-evolution behaviors: starting from the high-T paramagnetic (PM) phase, the system evolves into the DS regime [second row of Fig. 1(c)], where the intradimer correlation $C_D = -\langle \mathbf{S}_i \cdot \mathbf{S}_j \rangle_D$ [cf. inset in Fig. 2(c)] is strongest and the spin structure factor peaks at X and Y points in the first Brillouin zone. Further decreasing temperature, it enters the plaquette liquid (PL) phase via a first-order transition, where C_D changes its sign and the interdimer correlation $C_{NN} = -\langle \mathbf{S}_i \cdot \mathbf{S}_j \rangle_{NN}$ [see also inset in Fig. 2(c)] becomes stronger, as shown in the third row of Fig. 1(c). In the PM, DS, and PL regimes, the equivalent NN bonds take the same values and there is no $\mathbb{Z}_2$ symmetry breaking; while at sufficiently low temperatures ($T < T_P^*$), the PL phase eventually gives way to the ordered

PS phase upon a second-order transition. The PS order can be detected by comparing two bonds with the same orientation [58], as shown in the last row of Fig. 1(c). Correspondingly, the spin structure peak shifts to the M point in the PL and ordered PS phases, with the latter being brighter. Markedly, this interesting temperature evolution of spin states due to the slightly bent first-order line is consistent with the results in a recent NMR experiment, where a phase coexistence phenomenon was observed [32].

First-order line and critical point.—We determine the critical point (CP), $(\alpha_c^*, T_c^*/J') \simeq (0.678, 0.036)$, in Fig. 1(a) as the position where two dashed lines, T_{DS} and T_{PL}, and the solid line T_1 meet. The latter, i.e., a first-order transition line, can be understood from intradimer correlation C_{D}, which serves as the corresponding density-type order parameter. As shown in Fig. 2(a), for $T < T_c^*$, a discontinuous jump in C_{D} occurs at $\alpha_1 \simeq 0.675$, a characteristic of the first-order transition between the DS and PL/PS phase. In contrast, for $T > T_c^*$, the simulated C_{D} data show a smooth change, which resembles that of liquid-gas crossover in the supercritical regime of water's pressure-temperature phase diagram [31]. According to the couplings determined in Refs. [28,30], our results correspond to a critical pressure around 2 GPa, and a critical temperature T_c^* about 2–3 K, in agreement with recent experiments [31]. We further examine the correlation jump between the DS and PS states $\Delta C_{\mathrm{D}} \sim [(T_c^* - T)/T_c^*]^{\beta}$ near the CP (from below) [31], with the fitted critical exponent $\beta \approx 1/8$ [36] falling into the two-dimensional Ising universality class. Notably, the white line in Fig. 2(a) with $C_{\mathrm{D}} \approx 0$, which roughly coincides with the T_{PL} line determined independently from the broad peak of C_m/T, indicates a *sign switching* in the intradimer correlations, as also observed experimentally [47].

In Fig. 1(a), there are two crossover temperature scales, T_{DS} and T_{PL}, determined from C_m/T humps. They can be elucidated by examining two types of local correlations, i.e., the interdimer C_{NN} and the intradimer C_{D}. As shown in Figs. 2(c) and 2(d), a shoulderlike structure is first developed in C_m/T at $T_{\mathrm{h}} \sim 0.4J'$, where both correlations build up with similar strengths. However, it is found that for $\alpha = 0.67 < \alpha_1$, [cf. Fig. 2(c)], the intra(inter) dimer correlations increase (decrease) rapidly around T_{DS}; while, for $\alpha = 0.68 > \alpha_1$, [cf. Fig. 2(d)], the situation around T_{PL} is reversed. Moreover, we define the empty PS order parameter $\mathcal{O}_{\mathrm{E}} \equiv \sum_i [(-1)^{i_x} \mathbf{S}_i \cdot \mathbf{S}_{i+\hat{x}} - (-1)^{i_y} \mathbf{S}_i \cdot \mathbf{S}_{i+\hat{y}}]$, with $i_{x,y}$ the coordinates of site i [cf. Fig. 1(b)], and the summation runs over sites of the central unit cell to alleviate finite-size effect. It is found that $\mathcal{O}_{\mathrm{E}}$ remains vanishingly small till near T_{P}^*, indicating the fluctuating plaquette order in the PL regime yet without $\mathbb{Z}_2$ symmetry breaking.

Second-order line and critical end point.—When further decreasing temperature, the specific heat peak gets brighter and becomes maximal at $(\alpha_{\mathrm{E}}, T_{\mathrm{E}}/J') \approx (0.674, 0.008)$, as shown in Fig. 1(a), which is nothing but the critical end point (CEP) [59,60]. On the right hand side of this point, there is a second-order thermal transition line T_{P}^* defined by the peaks of C_m/T, which goes downward and eventually drops outside of our temperature window when approaching the possible QPT at $\alpha_2^* \approx 0.692$ determined by DMRG calculations [36]. Such a peak structure has been experimentally observed recently [30,31]. Here, we perform low-temperature calculations down to the previously inaccessible regime [21,31,48,49], and identify the ordered PS phase below the transition temperature $T_{\mathrm{P}}^* \sim 0.01J'$, i.e., resembling the "solid" or "ice" beneath the "liquid" phase in the water's phase diagram. The low-temperature calculations smoothly extrapolate to the ground-state DMRG results, and hence provide a *comprehensive* pressure-temperature phase diagram of the SS model in Fig. 1(a). Noteworthily, although the PS order transition found experimentally is around $T/J' \sim 0.02$ [30,31], slightly higher than the value obtained here for $W = 6$ geometry, our finite-size analysis indicates that T_{P}^* increases with width, and the rudimentary width-8 result of T_{P}^* already takes a similar value (cf. Supplemental Material, Fig. S2 [36]).

To understand the nature of this low-temperature PS phase, in particular, whether the symmetry breaking occurs among the empty or full plaquettes, we compute order parameters for both the empty ($\mathcal{O}_{\mathrm{E}}$) and full ($\mathcal{O}_{\mathrm{F}}$) PS states. The former is shown in Figs. 2(b)–2(d), while the latter is found to be much smaller (see more details in Supplemental Material, Sec. III B [36]). In Fig. 2(d), we find $\mathcal{O}_{\mathrm{E}}$ remains zero until around T_{P}^*, where the specific heat shows a peak. It corresponds to the rapid buildup of $\mathbb{Z}_2$ symmetry breaking order amongst empty plaquettes. We also compute the PS susceptibility for both empty (χ_{E}) and full (χ_{F}) PS orders, and find that the former increases much faster even in the PL regime below T_{PL} [36]. Therefore, we conclude that the empty PS instability predominates over the full one in the entire low-temperature range, and confirm that the PS phase is of empty type in the pressure-temperature phase diagram. Since recent experiments indicate instead the full-plaquette state in $SrCu_2(BO_3)_2$ [28,32,47], one needs to consider additional terms beyond the basic SSM to resolve this subtle discrepancy [19].

Supercritical regime and magnetic barocalorics.—It is well known that water in its supercritical state has many fascinating physical properties leading to various applications [61]. In the case of quantum magnets, the supercritical regime remains largely unexplored [62]. Here, we initiate the investigation of supercriticality in the SS model from the perspective of magnetothermodynamics. In Fig. 3(a), we present the isentropes in this regime, where a prominent adiabatic magnetic cooling effect is found. By connecting the lowest temperature points of isentropes, we obtain a maximal entropy line with strong spin fluctuations that resembles the renowned Widom line in the supercritical regime [63]. As such a cooling effect originates from the magnetic entropy change and is controlled by pressure, we dub it magnetic barocaloric effect, and propose to characterize it by a

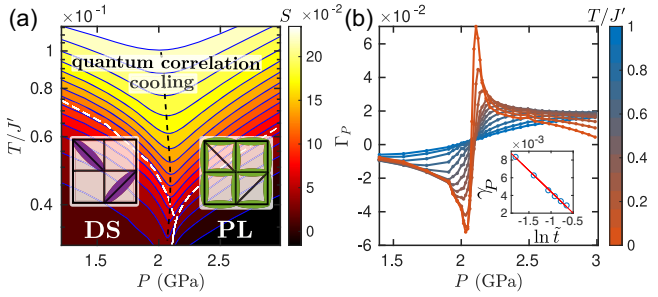

FIG. 3. (a) Contour plot of thermal entropy S with isentropes indicated by blue solid lines, where a prominent cooling effect due to dramatic change in quantum correlations is observed. The white dashed and solid lines are determined from C_m/T [cf. Fig. 1(a)]. The black dashed line connects the dips of isentropes and represents a line of maximal entropy. (b) Grüneisen ratio Γ_P vs pressure P. The inset shows $\gamma_P(\tilde{t})$ vs $\ln\tilde{t} \equiv \ln[(T-T_c^*)/T_c^*]$ (blue circles), with the fitting (red line) also shown. In both panels, we use the relation between coupling strength and pressure given by [28], i.e., $J'(P) = (75 - 8.3P/\mathrm{GPa})$ K and $J(P) = (46.7 - 3.7P/\mathrm{GPa})$ K.

Grüneisen ratio $\Gamma_P \equiv -(1/T)\{[(\partial S/\partial P)_T]/[(\partial S/\partial T)_P]\}$. As shown in Fig. 3(b), a clear sign change with very pronounced peak/dip can be observed in Γ_P for supercritical spin states. More specifically, we denote the nominator by $\gamma_P \equiv -(\partial S/\partial P)_T \sim \partial\langle \mathbf{S}_i \cdot \mathbf{S}_j\rangle/\partial T$, and find a universal scaling $\gamma_P \sim \ln[(T-T_c^*)/T_c^*]$ near the CP [cf. the inset of Fig. 3(b)], dictated by the 2D Ising universality class. Notably, in sharp distinction to the conventional magnetic cooling due to entropy change via an order-disorder switch of the magnetic moment's orientations [64], here the magnetic barocaloric effect is related to the rearrangements in spin singlet patterns [illustrated in the inset of Fig. 3(a)]. Such a quantum correlation induced cooling, observed in the supercritical regime and ascribed to the rearrangement of disorder singlet patterns, constitutes a novel mechanism for helium-free cryogenics.

Field-temperature phase diagram and spin-supersolid transition.—Given the ordered PS phase identified, we consider applying magnetic fields to pressured $SrCu_2(BO_3)_2$ [32,33] along the spin S^z direction, i.e., $H \to H - h\sum_i S_i^z$. Here, we focus on $J/J' = 0.68$ and $h/J' \le 0.25$, and the contour plot of C_m/T is shown in Fig. 4(a), where we find both temperature scales, T_{PL} and T_P^*, decrease as the field increases, and the latter will eventually drop out of the available temperature window. A low-temperature C_m/T peak reappears for $h/J' \gtrsim 0.22$, suggesting a QPT occurs before $h/J' = 0.22$.

To clarify the quantum phases and phase transitions in Fig. 4(a), we perform DMRG calculations and show the results in Figs. 4(b) and 4(c). On width-6 cylinder, there exists a pressure-induced intermediate PS phase [20], which gives way to a stripy SSS [33] phase for $h > h_c/J' \simeq 0.185$ [cf. Fig. 4(b)] via a QPT possibly of first order [36]. In the SSS phase with $h/J' = 0.2$, we show the computed

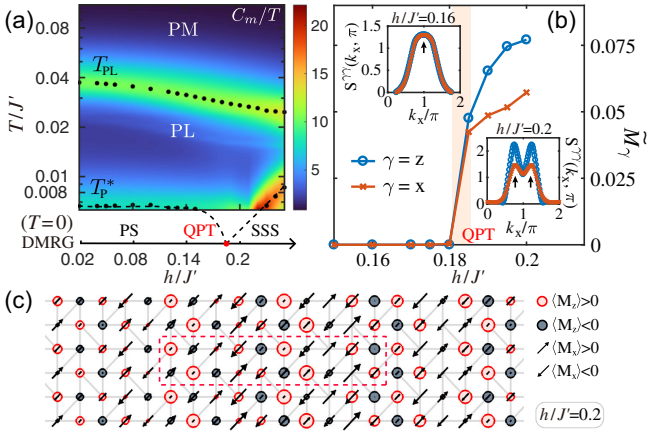

FIG. 4. (a) Contour plot of C_m/T with black dots indicating locations of the peaks, which extrapolate to the ground-state phase diagram where a QPT occurs at $h_c/J' \simeq 0.185$ (for $J/J' = 0.68$). (b) The "solid" and "superfluid" spin order parameters $\tilde{M}_\gamma$ $(\gamma = x,\ z)$ computed as $(1/N_{\mathrm{bulk}})\sum_{i\in\mathrm{bulk}}|\langle M_\gamma\rangle_i|$ with site i running over bulk of the cylinder. The insets show the spin-structure factors $S^{zz}(k_x,k_y)$ and $S^{xx}(k_x,k_y)$, under two different fields $h/J' = 0.16$ and 0.2. (c) Spin texture in the SSS phase, where the moments are displayed with the longitudinal ($\langle M_z\rangle_i$) and transverse ($\langle M_x\rangle_i$) magnetic moments. The positive (negative) $\langle M_z\rangle_i$ values are illustrated with red (black) circles, and the $\langle M_x\rangle_i$ components with the arrows. The size of the circles and length of the arrows reflect the absolute values of corresponding local moments, where a 10×2 unit cell on a 6×30 cylinder is indicated by the red dashed box.

local moments in Fig. 4(c) where a 10×2 unit cell can be observed, similar to the previously iPEPS results [33]. In the SSS phase, both $\langle M_x\rangle$ and $\langle M_z\rangle$ are nonzero, indicating that both translational and U(1) symmetries are simultaneously broken, i.e., there exists a quantum magnetic analog of supersolidity. Taking $J' \approx 60$ K for $SrCu_2(BO_3)_2$ under pressure of about 2.0 GPa [30], we estimate the field-driven QPT takes place at $h_c \approx 8$ T, in agreement with recent experiments [32,33].

The SSS order is also evident in the spin structure factors $S^{\gamma\gamma}(\mathbf{k}) = N^{-1}\sum_{i,j} e^{-i\mathbf{k}\cdot(\mathbf{r}_i-\mathbf{r}_j)}\langle S_i^\gamma \cdot S_j^\gamma\rangle$ (with N the total lattice sites) shown in the insets of Fig. 4(b), where a broad peak in the PS phase changes into a double-peak structure split apart at $k_x = \pi \pm (\pi/5)$, as h changes from 0.16 to 0.2. Such a peak-splitting behavior is also found when decreasing temperature [36], accessible by neutron scattering measurements for probing the SSS phase. We note that for different choices of α, other phases may show up instead of SSS, making the field-driven spin states and transitions extremely rich in the pressured $SrCu_2(BO_3)_2$ [32,33].

Discussion and outlook.—Recent experimental advances [30–32] have added greatly to the understanding of the pressure-field-temperature phase diagram of $SrCu_2(BO_3)_2$, which advocate comprehensive theoretical studies. Here, with the state-of-the-art tensor-network approach, we map

out the finite-temperature phase diagram that explains experimental findings and opens a refreshing avenue in the $SrCu_2(BO_3)_2$ studies. In particular, the ordered PS phase and its thermal transition line are identified, and the nature of the *low-temperature* PS phase is clarified by finding that the empty PS order is always predominant over the full one at low temperature. This nails down the direction to explain the discrepancy, i.e., the original SS model could not fully capture the low-T phase in $SrCu_2(BO_3)_2$, and one might need to consider additional terms for the model Hamiltonian. As the PS transition takes place at very low temperature, i.e., $T_P^*/J' \sim O(0.01)$, it suggests that other (small) interactions, including the interlayer couplings ($\lesssim$10% of J' [65]), spin-orbit couplings (~3% [66]), distortion [19], and staggered ring exchange interaction [22], may be relevant to make a more pertinent theoretical explanation on $SrCu_2(BO_3)_2$. Moreover, we call for future experimental investigations of the magnetic barocaloric in the supercritical regime, which constitutes a *bona fide* spin correlation cooling effect fundamentally different from traditional magnetic refrigeration. The novel cooling mechanism in frustrated magnets enables potential applications in space cryogenics [67] and quantum technologies [68].

The pressure-driven PS-AFM quantum phase transition has been intensively studied recently [20,24,25]. Our finite-T studies here, for a width-6 system, find no salient feature near α_2^* in simulated quantities [36]. Whether this transition belongs to a DQCP [20] or is replaced by a quantum spin liquid phase [23–25] unfortunately cannot be addressed here. Instead, the field-driven PS-SSS transition in the case of $\alpha = 0.68$ (i.e., 2.2 GPa pressure in experiments) belongs to first order and can be probed by magnetocaloric measurements [36]. Meanwhile, a field-driven PS-AFM phase transition was recently observed under a relatively higher pressure (e.g., 2.4 GPa) and has been suggested to be a proximate DQCP [32], which remains for future studies.

J. W. and W. L. are indebted to Rong Yu, Ling Wang, Anders Sandvik, Zi Yang Meng, and Weiqiang Yu for stimulating discussions. This work was supported by the National Natural Science Foundation of China (Grants No. 12222412, No. 11834014, No. 11974036, and No. 12047503), National Key R&D Program of China (Grants No. 2018YFA0305800 and No. 2022YFA1402704), Strategic Priority Research Program of Chinese Academy of Sciences (CAS) (Grant No. XDB 28000000), the Fundamental Research Funds for the Central Universities, the CAS Project for Young Scientists in Basic Research (YSBR-003,YSBR-057), and the Innovation Program for Quantum Science and Technology (under Grant No. 2021ZD0301900). We thank the HPC-ITP for the technical support and generous allocation of CPU time.

*These authors contributed equally to this work.
†yan@ucas.ac.cn
‡w.li@itp.ac.cn
§gsu@ucas.ac.cn

[1] *Introduction to Frustrated Magnetism*, edited by C. Lacroix, P. Mendels, and F. Mila (Springer, Berlin, Heidelberg, 2011).
[2] H. T. Diep, *Frustrated Spin Systems*, 3rd ed. (World Scientific, Singapore, 2020).
[3] L. Balents, Spin liquids in frustrated magnets, Nature (London) **464**, 199 (2010).
[4] Y. Zhou, K. Kanoda, and T.-K. Ng, Quantum spin liquid states, Rev. Mod. Phys. **89**, 025003 (2017).
[5] C. Broholm, R. J. Cava, S. A. Kivelson, D. G. Nocera, M. R. Norman, and T. Senthil, Quantum spin liquids, Science **367**, eaay0668 (2020).
[6] T. Senthil, A. Vishwanath, L. Balents, S. Sachdev, and M. P. A. Fisher, Deconfined quantum critical points, Science **303**, 1490 (2004).
[7] B. S. Shastry and B. Sutherland, Exact ground state of a quantum mechanical antiferromagnet, Physica (Amsterdam) **108B+C**, 1069 (1981).
[8] M. Albrecht and F. Mila, First-order transition between magnetic order and valence bond order in a 2D frustrated Heisenberg model, Europhys. Lett. **34**, 145 (1996).
[9] S. Miyahara and K. Ueda, Exact Dimer Ground State of the Two Dimensional Heisenberg Spin System $SrCu_2(BO_3)_2$, Phys. Rev. Lett. **82**, 3701 (1999).
[10] E. Müller–Hartmann, R. R. P. Singh, C. Knetter, and G. S. Uhrig, Exact Demonstration of Magnetization Plateaus and First-Order Dimer-Néel Phase Transitions in a Modified Shastry-Sutherland Model for $SrCu_2(BO_3)_2$, Phys. Rev. Lett. **84**, 1808 (2000).
[11] A. Koga and N. Kawakami, Quantum Phase Transitions in the Shastry-Sutherland Model for $SrCu_2(BO_3)_2$, Phys. Rev. Lett. **84**, 4461 (2000).
[12] W. Zheng, J. Oitmaa, and C. J. Hamer, Phase diagram of the Shastry-Sutherland antiferromagnet, Phys. Rev. B **65**, 014408 (2001).
[13] Y. Takushima, A. Koga, and N. Kawakami, Competing spin-gap phases in a frustrated quantum spin system in two dimensions, J. Phys. Soc. Jpn. **70**, 1369 (2001).
[14] C. H. Chung, J. B. Marston, and S. Sachdev, Quantum phases of the Shastry-Sutherland antiferromagnet: Application to $SrCu_2(BO_3)_2$, Phys. Rev. B **64**, 134407 (2001).
[15] A. Läuchli, S. Wessel, and M. Sigrist, Phase diagram of the quadrumerized Shastry-Sutherland model, Phys. Rev. B **66**, 014401 (2002).
[16] A. Isacsson and O. F. Syljuåsen, Variational treatment of the Shastry-Sutherland antiferromagnet using projected entangled pair states, Phys. Rev. E **74**, 026701 (2006).
[17] J. Lou, T. Suzuki, K. Harada, and N. Kawashima, Study of the Shastry Sutherland model using multi-scale entanglement renormalization ansatz, arXiv:1212.1999v1.
[18] P. Corboz and F. Mila, Tensor network study of the Shastry-Sutherland model in zero magnetic field, Phys. Rev. B **87**, 115144 (2013).
[19] C. Boos, S. P. G. Crone, I. A. Niesen, P. Corboz, K. P. Schmidt, and F. Mila, Competition between intermediate plaquette phases in $SrCu_2(BO_3)_2$ under pressure, Phys. Rev. B **100**, 140413(R) (2019).

[20] J. Y. Lee, Y.-Z. You, S. Sachdev, and A. Vishwanath, Signatures of a Deconfined Phase Transition on the Shastry-Sutherland Lattice: Applications to Quantum Critical $SrCu_2(BO_3)_2$, Phys. Rev. X **9**, 041037 (2019).

[21] T. Shimokawa, Signatures of finite-temperature mirror symmetry breaking in the $S = \frac{1}{2}$ Shastry-Sutherland model, Phys. Rev. B **103**, 134419 (2021).

[22] N. Xi, H. Chen, Z. Y. Xie, and R. Yu, Plaquette valence bond solid to antiferromagnet transition and deconfined quantum critical point of the Shastry-Sutherland model, Phys. Rev. B **107**, L220408 (2023).

[23] A. Keles and E. Zhao, Rise and fall of plaquette order in the Shastry-Sutherland magnet revealed by pseudofermion functional renormalization group, Phys. Rev. B **105**, L041115 (2022).

[24] L. Wang, Y. Zhang, and A. W. Sandvik, Quantum spin liquid phase in the Shastry-Sutherland model detected by an improved level spectroscopic method, Chin. Phys. Lett. **39**, 077502 (2022).

[25] J. Yang, A. W. Sandvik, and L. Wang, Quantum criticality and spin liquid phase in the Shastry-Sutherland model, Phys. Rev. B **105**, L060409 (2022).

[26] H. Kageyama, K. Yoshimura, R. Stern, N. V. Mushnikov, K. Onizuka, M. Kato, K. Kosuge, C. P. Slichter, T. Goto, and Y. Ueda, Exact Dimer Ground State and Quantized Magnetization Plateaus in the Two-Dimensional Spin System $SrCu_2(BO_3)_2$, Phys. Rev. Lett. **82**, 3168 (1999).

[27] G. Radtke, A. Saúl, H. A. Dabkowska, M. B. Salamon, and M. Jaime, Magnetic nanopantograph in the $SrCu_2(BO_3)_2$ Shastry-Sutherland lattice, Proc. Natl. Acad. Sci. U.S.A. **112**, 1971 (2015).

[28] M. E. Zayed, C. Rüegg, J. J. Larrea, A. M. Läuchli, C. Panagopoulos, S. S. Saxena, M. Ellerby, D. F. McMorrow, T. Strässle, S. Klotz, G. Hamel, R. A. Sadykov, V. Pomjakushin, M. Boehm, M. Jiménez–Ruiz, A. Schneidewind, E. Pomjakushina, M. Stingaciu, K. Conder, and H. M. Rønnow, 4-spin plaquette singlet state in the Shastry–Sutherland compound $SrCu_2(BO_3)_2$, Nat. Phys. **13**, 962 (2017).

[29] P. A. McClarty, F. Krüger, T. Guidi, S. F. Parker, K. Refson, A. W. Parker, D. Prabhakaran, and R. Coldea, Topological triplon modes and bound states in a Shastry-Sutherland magnet, Nat. Phys. **13**, 736 (2017).

[30] J. Guo, G. Sun, B. Zhao, L. Wang, W. Hong, V. A. Sidorov, N. Ma, Q. Wu, S. Li, Z. Y. Meng, A. W. Sandvik, and L. Sun, Quantum Phases of $SrCu_2(BO_3)_2$ from High-Pressure Thermodynamics, Phys. Rev. Lett. **124**, 206602 (2020).

[31] J. L. Jiménez, S. P. G. Crone, E. Fogh, M. E. Zayed, R. Lortz, E. Pomjakushina, K. Conder, A. M. Läuchli, L. Weber, S. Wessel, A. Honecker, B. Normand, C. Rüegg, P. Corboz, H. M. Rønnow, and F. Mila, A quantum magnetic analogue to the critical point of water, Nature (London) **592**, 370 (2021).

[32] Y. Cui, L. Liu, H. Lin, K.-H. Wu, W. Hong, X. Liu, C. Li, Z. Hu, N. Xi, S. Li, R. Yu, A. W. Sandvik, and W. Yu, Proximate deconfined quantum critical point in $SrCu_2(BO_3)_2$, Science **380**, 1179 (2023).

[33] Z. Shi, S. Dissanayake, P. Corboz, W. Steinhardt, D. Graf, D. M. Silevitch, H. A. Dabkowska, T. F. Rosenbaum, F. Mila, and S. Haravifard, Discovery of quantum phases in the Shastry-Sutherland compound $SrCu_2(BO_3)_2$ under extreme conditions of field and pressure, Nat. Commun. **13**, 2301 (2022).

[34] T. Nomura, P. Corboz, A. Miyata, S. Zherlitsyn, Y. Ishii, Y. Kohama, Y. H. Matsuda, A. Ikeda, C. Zhong, H. Kageyama, and F. Mila, The Shastry-Sutherland compound $SrCu_2(BO_3)_2$ studied up to the saturation magnetic field, Nat. Commun. **14**, 3769 (2023).

[35] E. Manousakis, The spin-½ Heisenberg antiferromagnet on a square lattice and its application to the cuprous oxides, Rev. Mod. Phys. **63**, 1 (1991).

[36] See Supplemental Material at http://link.aps.org/supplemental/10.1103/PhysRevLett.131.116702 for details on (i) finite-temperature tensor renormalization group, (ii) density matrix renormalization group simulations, and more results on the SSM (iii) in zero magnetic field as well as (iv) finite fields, which additionally includes Refs. [37–46].

[37] Q. Li, Y. Gao, Y.-Y. He, Y. Qi, B.-B. Chen, and W. Li, Tangent Space Approach for Thermal Tensor Network Simulations of the 2D Hubbard Model, Phys. Rev. Lett. **130**, 226502 (2023).

[38] Yuan Gao, Qiaoyi Li, Han Li, Junsen Wang, Gang Su, and Wei Li (to be published).

[39] E. M. Stoudenmire and S. R. White, Studying two-dimensional systems with the density matrix renormalization group, Annu. Rev. Condens. Matter Phys. **3**, 111 (2012).

[40] A. Weichselbaum, Non-Abelian symmetries in tensor networks: A quantum symmetry space approach, Ann. Phys. (Amsterdam) **327**, 2972 (2012).

[41] A. Weichselbaum, X-symbols for non-Abelian symmetries in tensor networks, Phys. Rev. Res. **2**, 023385 (2020).

[42] Y.-L. Dong, L. Chen, Y.-J. Liu, and W. Li, Bilayer linearized tensor renormalization group approach for thermal tensor networks, Phys. Rev. B **95**, 144428 (2017).

[43] L. Zhu, M. Garst, A. Rosch, and Q. Si, Universally Diverging Grüneisen Parameter and the Magnetocaloric Effect Close to Quantum Critical Points, Phys. Rev. Lett. **91**, 066404 (2003).

[44] M. Garst and A. Rosch, Sign change of the Grüneisen parameter and magnetocaloric effect near quantum critical points, Phys. Rev. B **72**, 205129 (2005).

[45] J. Haegeman, C. Lubich, I. Oseledets, B. Vandereycken, and F. Verstraete, Unifying time evolution and optimization with matrix product states, Phys. Rev. B **94**, 165116 (2016).

[46] J. Haegeman, J. I. Cirac, T. J. Osborne, I. Pižorn, H. Verschelde, and F. Verstraete, Time-Dependent Variational Principle for Quantum Lattices, Phys. Rev. Lett. **107**, 070601 (2011).

[47] S. Bettler, L. Stoppel, Z. Yan, S. Gvasaliya, and A. Zheludev, Sign switching of dimer correlations in $SrCu_2(BO_3)_2$ under hydrostatic pressure, Phys. Rev. Res. **2**, 012010(R) (2020).

[48] S. Wessel, I. Niesen, J. Stapmanns, B. Normand, F. Mila, P. Corboz, and A. Honecker, Thermodynamic properties of the Shastry-Sutherland model from quantum Monte Carlo simulations, Phys. Rev. B **98**, 174432 (2018).

[49] A. Wietek, P. Corboz, S. Wessel, B. Normand, F. Mila, and A. Honecker, Thermodynamic properties of the

Shastry-Sutherland model throughout the dimer-product phase, Phys. Rev. Res. **1**, 033038 (2019).
[50] B.-B. Chen, Y.-J. Liu, Z. Chen, and W. Li, Series-expansion thermal tensor network approach for quantum lattice models, Phys. Rev. B **95**, 161104(R) (2017).
[51] B.-B. Chen, L. Chen, Z. Chen, W. Li, and A. Weichselbaum, Exponential Thermal Tensor Network Approach for Quantum Lattice Models, Phys. Rev. X **8**, 031082 (2018).
[52] H. Li, B.-B. Chen, Z. Chen, J. von Delft, A. Weichselbaum, and W. Li, Thermal tensor renormalization group simulations of square-lattice quantum spin models, Phys. Rev. B **100**, 045110 (2019).
[53] H. Li, Y.-D. Liao, B.-B. Chen, X.-T. Zeng, X.-L. Sheng, Y. Qi, Z. Y. Meng, and W. Li, Kosterlitz-Thouless melting of magnetic order in the triangular quantum Ising material $TmMgGaO_4$, Nat. Commun. **11**, 1111 (2020).
[54] H. Li, H.-K. Zhang, J. Wang, H.-Q. Wu, Y. Gao, D.-W. Qu, Z.-X. Liu, S.-S. Gong, and W. Li, Identification of magnetic interactions and high-field quantum spin liquid in α-$RuCl_3$, Nat. Commun. **12**, 4007 (2021).
[55] S. Yu, Y. Gao, B.-B. Chen, and W. Li, Learning the effective spin Hamiltonian of a quantum magnet, Chin. Phys. Lett. **38**, 097502 (2021).
[56] Y. Gao, Y.-C. Fan, H. Li, F. Yang, X.-T. Zeng, X.-L. Sheng, R. Zhong, Y. Qi, Y. Wan, and W. Li, Spin supersolidity in nearly ideal easy-axis triangular quantum antiferromagnet $Na_2BaCo(PO_4)_2$, npj Quantum Mater. **7**, 89 (2022).
[57] S. R. White, Density Matrix Formulation for Quantum Renormalization Groups, Phys. Rev. Lett. **69**, 2863 (1992).
[58] The cylinder boundary condition introduces an effective pinning field that may favour a particular plaquette pattern [25], and in practice we measure the order parameters in the central unit cell as elaborated in [36].
[59] M. E. Fisher and P. J. Upton, Universality and Interfaces at Critical End Points, Phys. Rev. Lett. **65**, 2402 (1990).
[60] M. E. Fisher and M. C. Barbosa, Phase boundaries near critical end points. I. Thermodynamics and universality, Phys. Rev. B **43**, 11177 (1991).
[61] A. A. Clifford and J. R. Williams, Introduction to supercritical fluids and their applications, in *Supercritical Fluid Methods and Protocols*, edited by J. R. Williams and A. A. Clifford (Humana Press, Totowa, NJ, 2000), pp. 1–16.
[62] L. Weber, A. Honecker, B. Normand, P. Corboz, F. Mila, and S. Wessel, Quantum Monte Carlo simulations in the trimer basis: First-order transitions and thermal critical points in frustrated trilayer magnets, SciPost Phys. **12**, 054 (2022).
[63] J. Luo, L. Xu, E. Lascaris, H. E. Stanley, and S. V. Buldyrev, Behavior of the Widom Line in Critical Phenomena, Phys. Rev. Lett. **112**, 135701 (2014).
[64] N. A. de Oliveira, P. J. von Ranke, and A. Troper, Magnetocaloric and barocaloric effects: Theoretical description and trends, Int. J. Refrig. **37**, 237 (2014).
[65] S. Miyahara and K. Ueda, Theory of the orthogonal dimer Heisenberg spin model for $SrCu_2(BO_3)_2$, J. Phys. Condens. Matter **15**, R327 (2003).
[66] H. Nojiri, H. Kageyama, Y. Ueda, and M. Motokawa, ESR study on the excited state energy spectrum of $SrCu_2(BO_3)_2$—A central role of multiple-triplet bound states, J. Phys. Soc. Jpn. **72**, 3243 (2003).
[67] P. J. Shirron, Applications of the magnetocaloric effect in single-stage, multi-stage and continuous adiabatic demagnetization refrigerators, Cryogenics **62**, 130 (2014).
[68] A. E. Jahromi, P. J. Shirron, and M. J. DiPirro, *Sub-Kelvin Cooling Systems for Quantum Computers*, Technical Report (NASA Goddard Space Flight Center Greenbelt, Maryland, 2019).